Wideband Off-Body Measurements and Channel Modeling at 60 GHz

Luca Petrillo, Theodoros Mavridis, Julien Sarrazin, Aziz Benlarbi-Delai, Philippe de Doncker

Wideband Off-Body Measurements and Channel Modeling at 60 GHz

Luca Petrillo, Theodoros Mavridis, Julien Sarrazin, *Member, IEEE*, Aziz Benlarbi-Delaï, Philippe De Doncker

***Abstract*—A wideband indoor channel model between an external base station and a worn receiver on the user body at 60 GHz has been developed based on indoor measurements. The results are presented for three different receiver locations: head, wrist, and belt. A Saleh-Valenzuela impulse response is proposed as numerical model for this scenario. Also path loss and delay spread results are driven out in order to discuss the node location for assessing an off-body communication.**

***Index Terms*—Body Area Networks, Millimeter waves, 60 GHz, V-Band, Off-Body**

I. Introduction

Many emerging technologies aiming at realizing short-range indoor communications with data rates of a few Gbit/s are working in the 60 GHz band [1]. The progress in low-cost full-band circuit design, and the wide available spectrum at 60 GHz will allow one to develop new communication services [2]. However, millimeter frequencies suffer from high propagation losses in free-space. Also, the human body proximity can create high losses and signal fading. Before implementing and optimizing these systems, it is necessary to model propagation for different scenarios such as the communication between two devices worn on the human body (on-body propagation) or the communication between an external base station and a body worn device (off-body propagation).

Analytic models for Body Area Networks can be obtained by using greatly simplified body geometries. The advantage of millimeter wave propagation modeling is the small skin depth, about 0.5 mm for the human body at 60 GHz, allowing one to consider a body model with only one layer. In [3], a flat body model is proposed, leading to Norton's equations while [4] models the body as a cylindrical cylinder filled with a material having the electric properties of the human skin. Experimental models have been proposed by [5], [6] for narrowband on-body communication. But, to the best knowledge of the authors, no model has been yet proposed for wideband 60 GHz off-body communications.

This paper proposes to measure and study the wideband off-body communication channel. The measurements are conducted in an indoor environment with different body orientations and antenna locations. The main contribution of the study is to emphasize how the location of the on-body antenna influences the wideband channel with respect to the total received power, the first path cluster and the multipath components. The second contribution is the cluster model of the first paths in LOS and NLOS scenarios, independently of the node.

L. Petrillo, T. Mavridis and P. De Doncker are with OPERA Dpt. - Wireless Communications Group, Université Libre de Bruxelles (ULB), B-1050 Brussels, Belgium e-mail: (tmavridi@ulb.ac.be ; lpetrillo@ulb.ac.be ; pdedonck@ulb.ac.be)

T. Mavridis, J. Sarrazin and A. Benlarbi-Delaï are with Sorbonne Universités, UPMC Univ Paris 06, UR2, L2E, F-75005, Paris, France e-mail: (julien.sarrazin@upmc.fr; aziz.benlarbi_delai@umpc.fr)

II. Channel Sounding

Different scenarios and links have been considered for off-body communications [7]. In this paper, we chose to focus on three specific nodes: Belt, Right Wrist and Right side of the Head. These nodes are both used for Body Area Networks and for mobile communications. The measurements were conducted in an indoor environment of 7 m $\times$ 4 m with a height of 2.5 m. The base station was at 1.2 m from the ground and the measurements have been conducted for three distances d between the transmitting antenna and the user body: 1, 2, and 3 m. For each distance d, the channel has been sampled for four body orientations: "front", "right side", "back" and "left side" with respect to the transmitter position. This makes a total of 12 scenarios for 3 different node positions creating 36 different channels.

Measurements of wideband off-body channels have been conducted using a Rhode & Schwarz ZVA Vector Network Analyzer up to 75 GHz with quasi omnidirectional antennas *FLANN Microwave* ref. MD249-AA. One antenna was attached to the body with elastic bands and was separated from the skin with a 10 mm slab of expanded polystyrene foam and polarized parallel to the base station antenna. The radio frequency at the VNA was swept from 58 to 62 GHz leading to a delay resolution of 0.25 ns. The sweep was performed over 401 equally-spaced frequency points allowing a maximal detectable delay of 100 ns. The VNA IF bandwidth has been set to 2 kHz leading to a 200 ms channel acquisition time. For each scenario (link-distance-orientation), hundred channel measurements have been performed. The antennas were placed vertically with respect to the ground. A 30 dB low noise amplifier was used at the receiving side in order to increase the dynamic range. A low attenuation coaxial cable (6 dB/m) was placed at the receiving side. It has been carefully checked that the S_{11} of the antenna remains below -10 dB for each scenario over the operating bandwidth.

During the measurements, the body was as static as possible in a standing position. The subject under study is a male of 1.85 m height, 75 kg mass, and 93 cm body perimeter.

III. Measurements Results

Analysis of the measurements has been done in the time domain. The time domain was obtained by using a Hamming

TABLE I
PATH GAIN AND RMS DELAY SPREAD.

Distance [m]	G [dB], σ_T [ns]					
	Belt		Wrist		Head	
	LOS	NLOS	LOS	NLOS	LOS	NLOS
1	-90.1 9.93	-101.4 22.82	-70.9 4.30	-82.7 9.38	-70.5 3.89	-85.5 9.79
2	-95.1 12.59	-97.4 17.80	-73.9 4.09	-81.9 7.87	-74.8 5.28	-84.0 9.07
3	-106.4 27.56	-102.2 25.51	-77.3 5.41	-82.4 6.30	-76.1 5.87	-84.5 8.44

window in order to reduce side lobes as proposed by [8]. In the following, the measured frequency response will be noted $H(f)$ and the associated impulse response $h(\tau)$ where:

$$h(\tau) = \mathcal{F}^{-1}\{H(f) \cdot \text{Hamming}(f)\} \tag{1}$$

Hamming(f) stands for a Hamming window, f is the frequency, τ is the excess delay, and $\mathcal{F}^{-1}$ is the inverse Fourier transform. The power delay profile (PDP) is commonly used to characterize the impulse response [8]. It is defined as:

$$\text{PDP}(\tau) = E\left[|h(\tau)|^2\right] \tag{2}$$

where the expected value $E[\cdot]$ is obtained by averaging over the impulse channel acquisitions. For sake of clarity, the different scenarios (front, left and right sides, and back) are summarized into line-of-sight (LOS) and non-LOS (NLOS) cases. The results have been split into these categories by studying the first path of the PDP. We defined the wideband Path Gain G as the total power of PDP:

$$G = \int_0^\infty \text{PDP}(\tau)\text{d}\tau. \tag{3}$$

Table I shows that G is always the lowest at "Belt" node. G at the two other nodes has similar values. The PDP also allows one to calculate the root mean square (rms) delay spread σ_τ:

$$\sigma_\tau = \sqrt{\frac{1}{G}\int_0^\infty \tau^2 \text{PDP}(\tau)\text{d}\tau - \tau_m^2} \tag{4}$$

with $\tau_m = \frac{1}{G}\int_0^\infty \tau\text{PDP}(\tau)\text{d}\tau$. The values of σ_τ are summarized in Table I. It shows that σ_τ is higher for the "Belt" node. This is due to a higher body shadowing leading to a more attenuated first path with respect to the multipath components as will be shown in the next sections. Also, it will be shown that "Head" and "Wrist" nodes are equivalent (as can be observed in Table I).

IV. FIRST PATH MODEL

In the following, we propose a separate analysis of the PDP of the first path since it has a strong influence on the channel. The analysis is performed on its power, its fading, and shape.

TABLE II
SUMMARY OF THE FIRST TAP MODEL.

		Line-of-Sight	Non-Line-of-Sight
P_{first} (AVG,STD) [dB]	Belt	(-100.36, 6.85)	(-123.07, 2.47)
	Wrist	(-78.39, 4.81)	(-97.10, 6.09)
	Head	(-75.65, 3.28)	(-100.33,7.68)
Fading	Belt	LogN. (mse = 2.5E-4) $\mu = 0$ $\sigma = 0.41$	LogN. (mse = 8.1E-5) $\mu = 0$ $\sigma = 0.46$
	Wrist	LogN. (mse = 3.6E-4) $\mu = 0$ $\sigma = 0.26$	Weib. (mse = 2.3E-4) $A = 1.13$ $B = 1.87$
	Head	LogN. (mse = 9.8E-4) $\mu = 0$ $\sigma = 0.14$	Weib. (mse = 3.2E-4) $A = 1.13$ $B = 2.44$
PDP	K_0	0 dB	-1.84 dB
	γ_0	0.0717 ns/dB	0.2101 ns/dB
	σ_{cluster0}	2.05 dB	6.18 dB

A. Power

The first path power is defined here as

$$P_{\text{first}} = \text{PDP}(\tau = 0) \ \text{ in dB} \tag{5}$$

Path loss equations are often expressed with distance d. Since measurements have been conducted for only three distances, it is not relevant to establish a path loss for the first path with respect to the distance between the source and receiver. We propose here to aggregate (distance and orientation) the measurements for each node and to give an averaged path loss and a standard deviation, summarized in the first part of Table II.

It can be seen that the "Belt" node has always the lowest P_{first} while the "Wrist" and "Head" nodes have similar received power. Also in these measurements, the body was remaining quasi-static.

B. Fading Distribution

To obtain the first path amplitude distribution, the path loss is removed in each measurement set. Also, it is expected that the fading distribution is the same for all three distances between the transmitter and the body. Hence, the data of the three distances have been aggregated. A variety of statistical models can be used to fit an empirical fading distribution. For sake of clarity, we have reduced the results to the models that have obtained the best fitting results: "Lognormal" and "Weibull". Maximum Likelihood estimators were used as well as the Akaike information criterion (AIC). It allowed us to choose the best distribution fit through the Akaike weight w in %. The distribution with the higher w was chosen as described by [9]. The second part of Table II shows the best distribution parameters for each case. The mean squared error (MSE) between the experimental cumulative distribution functions and the models are also reported.

C. Power Delay Profile model

In Saleh-Valenzuela models, the power decay is commonly exponential with the excess delay. In [10] a generalized model

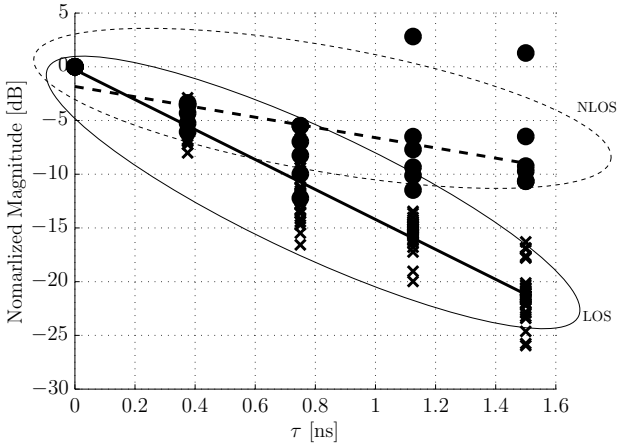

Fig. 1. PDP of the first path

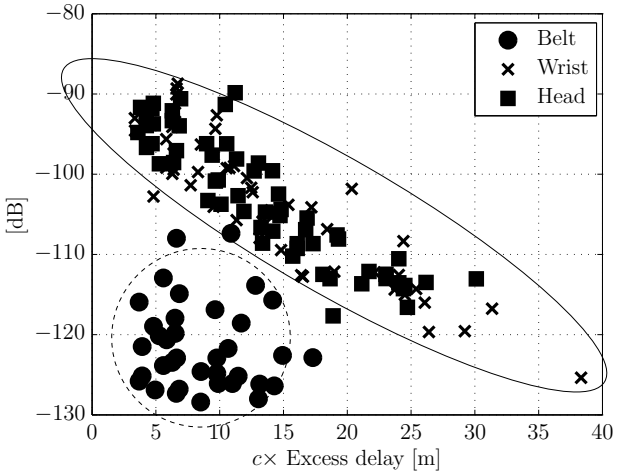

Fig. 2. Power of each cluster with the propagation distance.

can be found with the introduction of the K-factor of the spike + exponential model [11]:

$$P_{\text{cluster0}} = K_0 - \tau/\gamma_0 + \mathcal{N}(0, \sigma_{\text{cluster0}}) \qquad \tau > 0 \qquad (6)$$

where P_{cluster0} is the normalized power in [dB] of the first cluster, γ_0 refers to the decay factor of the first cluster, K_0 is the K-factor in dB and the variations are modeled by a normal distribution $\mathcal{N}$ of zero mean and standard deviation σ_{cluster0}. The PDPs are shown in Fig. 1.It is shown in [8] that the PDP shape differs for different orientations of the body in the UWB case. In regard of our experiments, we propose here to make an unified model depending on the LOS or NLOS configuration. The parameters obtained from the linear fit are summarized in the third part of Table II.

V. Multipath Components Model

A. Number of Clusters

Many algorithms have been proposed in order to identify the different clusters in a PDP [12]. However, these automated algorithms are not really convenient for the proposed scenario since the PDPs have different shapes (LOS or NLOS). Hence, the best way found by the authors (as in [13]) to distinguish the clusters is to do it manually based on a visual inspection.

Considering the number of scenarios (three distances $\times$ four body orientations) for each node position, the measurements do not allow one to draw an accurate distribution for the number of clusters. Some papers propose a fixed number of clusters [13] for each scenario which is inconvenient in our case. We propose to model the number of clusters as uniform between the minimum and maximum measured values which are summarized in the first two rows of Table III. Compared to similar scenarios where the human body is not involved [14], we found half the number of MPC clusters, because of the blockage of the human body and because we do not discriminate in our experiments the directions of arrival due to the quasi-omnidirectional antennas used.

B. Path Loss

The power in dB of the first tap of each cluster P_{MPC} is reported in Fig. 2 with the propagation distance calculated as the speed of light times the excess delay. MPC are reflected quasi-optically at 60 GHz by walls, ceiling, floor, and office furniture, often metallic. So, for example, propagation distance of MPC around 5 m corresponds to first-order reflections, while weaker MPCs with propagation distances between 10 and 15 m are more likely to be second order reflections. It can be seen that the "Wrist" and "Head" nodes present a linear decrease with the excess delay as expected, with values of the slope comparable to those found in scenarios where the human body is not involved [14], while the "Belt" node exhibits a scatter plot shape. This may be due to the higher blockage of the body for the "Belt" node. It is proposed to model the power of the MPCs in dB by a linear decrease with the excess delay for the 'Wrist" and "Head" nodes:

$$P_{\text{MPC}} = P^0_{\text{MPC}} - \tau/\Gamma + \mathcal{N}(0, \sigma_{\text{MPC}}) \qquad (7)$$

where P^0_{MPC} is the reference MPC power (obtained by fitting), Γ is the decay exponent and the variations are modelled by a normal distribution $\mathcal{N}$ of zero mean and standard deviation σ_{MPC}. It is assumed that the MPC power of the "Belt" node is independent of the delay. We propose in this case to model the MPC power by a normal distribution $\mathcal{N}(\mu, \sigma)$ with μ as mean value and σ as standard deviation. The numerical values are presented in the second part of Table III.

C. Cluster arrival time

Cluster arrival times T_l are studied using the time difference between consecutive arrival clusters $T_l - T_{l-1}$. Its distribution is given by an exponential law such that the conditional probability of arrival p is given by:

$$p(T_l|T_{l-1}) = \Lambda e^{-\Lambda(T_l - T_{l-1})} \qquad (8)$$

with Λ as the cluster arrival rate, $T_0 = 0$ and $l > 0$. The cluster arrival rate is also summarized in Table III.

TABLE III
MPC MODEL PARAMETERS SUMMARY.

	Parameter	Wrist	Head	Belt
Number of cluster	Min.	2	4	1
	Max.	6	6	5
Path Loss	P^0_{MPC} [dB]	-90.4	-89.1	$\mathcal{N}(-121.4, 5.42)$ [dB]
	Γ [ns/dB]	2.33	2.17	
	σ_{MPC}	3.87	3.58	
Time of Arrival	Λ [1/ns]	0.056	0.076	0.14
PDP	K_{cluster} [dB]	-0.59	-0.60	-0.57
	γ [ns/dB]	0.144	0.152	0.183
	σ_{cluster} [dB]	1.99	1.76	2.00

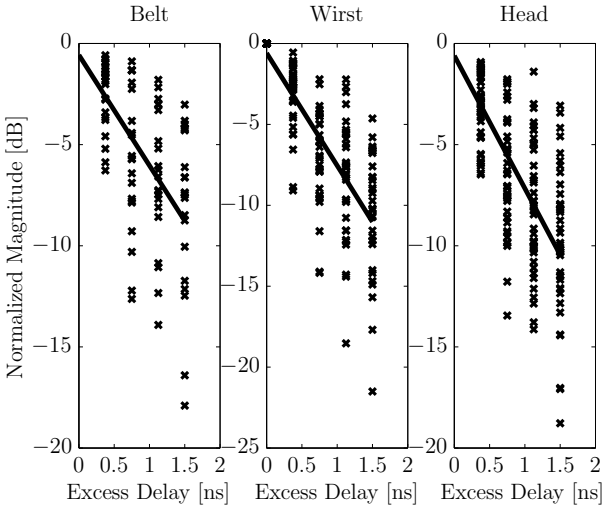

Fig. 3. Power Delay profile of each cluster with the excess delay. The dots are the measurement and the plain line is the best linear fit.

D. Power Delay Profile

It is found that all multipath components PDPs have a similar shape in the delay. In this case, each cluster is studied in Fig. 3 by shifting the measurement as $\tau_l = \tau - T_l$ and by normalizing the measurement as PDP$/P_{\text{MPC}}$:

$$P_{\text{cluster}} = K_{\text{cluster}} - \tau_l/\gamma + \mathcal{N}(0, \sigma_{\text{cluster}}) \qquad \tau_l > 0 \qquad (9)$$

Measured clusters are shown in Fig. 3 and fitted for $\tau_l > 0$ by a line as done in section IV-C. The parameters of (9) are summarized in the last rows of Table. III.

VI. Conclusion

This paper presents wideband channel measurements between an external base station and a node located on the body at 60 GHz. The receiver node is located at three different locations: belt, wrist, and head. The channels have been studied for four different body orientations with respect to the transmitter: front, back, right and left side. The measurements have been conducted in an indoor environment and for three different distances between the external base station and the body. An impulse response model has been proposed using a generalized Saleh-Valenzuela model.

The first cluster has been modeled in the LOS and NLOS cases. It has been shown that "Belt" node has always the lower power, while "Wrist" and "Head" nodes have similar powers. The power of the first cluster has been modeled by a lognormal distribution in the LOS case and in the NLOS case for the "Belt node", while a Weibull distribution has been found more appropriate to describe NLOS in "Wrist" and "Head" nodes. Finally, the shape of the first cluster presented a sharper decay for the LOS channels compared to NLOS. Approximately half the number of clusters was observed as compared to measurements found in the literature for equivalent scenarios not involving the human body. For "Wrist" and "Head" nodes, the power of each cluster decays linearly in logarithmic scale with the propagation distance as expected, while "Belt" node fails to exhibit such usual behavior.

VII. Acknowledgment

This work was performed within the Labex SMART supported by French state funds managed by the ANR-11-IDEX-0004-02. This work is also supported by grants of the FNRS (FRIA grant), Belgium.

References

[1] N. Guo *et al.*, "60-GHz Millimeter-Wave Radio: Principle, Technology, and New Results," *EURASIP J. Wireless Commun. Netw.*, 2007.
[2] S. K. Yong and C. C. Chong, "An Overview of Multigigabit Wireless through Millimeter Wave Technology: Potentials and Technical Challenges," *EURASIP J. Wireless Commun. Netw.*, 2006.
[3] N. Chahat *et al.*, "On-Body Propagation at 60 GHz," *IEEE Trans. Antennas Propag.*, vol. 61, no. 4, pp. 1876–1888, 2013.
[4] L. Petrillo *et al.*, "Analytical Creeping Wave Model and Measurements for 60 GHz Body Area Networks," *IEEE Trans. Antennas Propag.*, vol. 62, no. 8, pp. 4352–4356, 2014.
[5] Y. I. Nechayev *et al.*, "Millimetre-wave path-loss variability between two body-mounted monopole antennas," *IET Microw., Antennas Propag.*, vol. 7, no. 1, pp. 1–7, 2013.
[6] L. Petrillo *et al.*, "Statistical On-Body Measurement Results at 60 GHz," *IEEE Trans. Antennas Propag.*, vol. 63, no. 1, pp. 400–403, 2015.
[7] S. L. Cotton, R. D'Errico, and C. Oestges, "A Review of Radio Channel Models for Body Centric Communications," *Radio Science*, vol. 49, pp. 371–388, 2014.
[8] A. Fort *et al.*, "An ultra-wideband body area propagation channel model-from statistics to implementation," *IEEE Trans. Microw. Theory Techn.*, vol. 54, no. 4, pp. 1820–1826, 2006.
[9] H. Akaike, "Information theory and an extension of the maximum likelihood principle," in *Selected Papers of Hirotugu Akaike*. Springer, 1998, pp. 199–213.
[10] A. Maltsev *et al.*, "Channel Models for 60 GHz WLAN Systems," *IEEE 802.11 TGad document: IEEE 802.11-09/0334r8*, 2010.
[11] V. Erceg *et al.*, "A Model for the Multipath Delay Profile of Fixed Wireless Channels," *IEEE J. Sel. Areas Commun.*, vol. 17, no. 3, pp. 399–410, 1999.
[12] J. Chuang, S. Bashir, and D. Michelson, "Automated Identification of Clusters in UWB Channel Impulse Responses," in *Canadian Conf. Elect. Computer Eng., CCECE 2007*, 2007, pp. 761–764.
[13] A. Molisch, J. Foerster, and M. Pendergrass, "Channel Models for Ultrawideband Personal Area Networks," *IEEE Trans. Wirel. Commun.*, vol. 10, no. 6, pp. 14–21, 2003.
[14] C. Gustafson *et al.*, "On mm-Wave Multi-path Clustering and Channel Modeling," *IEEE Trans. Antennas Propag.*, vol. 62, no. 3, pp. 1445–1455, 2014.